

# Direct Imaging of the Structural Transition and Interconversion of Macroporous Bicontinuous Diamond-Surface Structure

Chao Bao<sup>a</sup>, Hao Chen<sup>b</sup>, Shunai Che<sup>a,c</sup> and Lu Han<sup>c,\*</sup>

<sup>a</sup> School of Chemistry and Chemical Engineering, State Key Laboratory of Metal Matrix Composites, Shanghai Key Laboratory for Molecular Engineering of Chiral Drugs, Shanghai Jiao Tong University 800 Dongchuan Road, Shanghai, 200240 (P.R. China)

<sup>b</sup> Institut für Numerische und Angewandte Mathematik, Georg-August-Universität Göttingen, Lotzestr. 16-18, Göttingen 37083, Germany

<sup>c</sup> School of Chemical Science and Engineering, Tongji University 1239 Siping Road, Shanghai, 200092 (P. R. China)

\* Corresponding author. E-mail addresses: luhan@tongji.edu.cn

## Abstract:

The porous solids with bicontinuous structures have received significant attention due to their complex structure with unique physical functionalities. They are often obtained through structural transformation from lamellae or cylindrical precursors. However, the experimental verification of this relationship is challenging due to the short life-span of the structural intermediates and the soft nature of the assembled amphiphilic systems. Herein, we report the observation of the structural change of macroporous bicontinuous diamond-surface structure in the self-assembly of block copolymeric system with inorganic precursors in a mixture solvent of tetrahydrofuran (THF) and HCl aqueous solution. By controlling the addition amount of HCl/H<sub>2</sub>O, both the electrostatic

interactions of the organic/inorganic precursor and the hydrolyzation and condensation rate of tetraethyl orthosilicate (TEOS) can be controlled. A structural transformation from bicontinuous diamond-surface to several intermediates between lamellar and bicontinuous structures has been observed with increasing the concentration of HCl. Our results show that the transition centers play an important role in the formation of the bicontinuous structure from the lamellae. Furthermore, we have proved the formation of interlamellar attachments (ILAs) and stalks as the intermediate phase. This study may bring new insights into the formation and the structural relationship of the bicontinuous porous solids and the corresponding relevant biological structures.

**Key words:** porous material, structural change, bicontinuous structure, lamellar, interlamellar attachments

## **1. Introduction:**

Many attempts have been carried out for fabricating ordered mesoporous and macroporous materials with ordered pore geometry, tunable pore size, controllable composition and large surface area with the aim for use in various applications.[1-8]

Among different structures of the porous solids, the bicontinuous structure have attracted tremendous interests due to their unique geometries and porous properties. The bicontinuous structures are consist

of two intertwining subvolumes separated by a non-self-intersecting intermediate layer. Three basic categories of triply periodic bicontinuous structures include the gyroid surface with space group  $Ia\bar{3}d$ , diamond surface with space group  $Pn\bar{3}m$ , and primitive surface, also known as “plumber's nightmare”, with space group  $Im\bar{3}m$ , respectively.[9]

In various natural and artificial synthesis systems, these structures and their analogies have been widely discovered, including mitochondrial membranes,[10] stressed or virally infected cells,[11, 12] biomineralized skeletons and scaffolds,[13-15] lyotropic and thermotropic liquid crystals[16-19] and their inorganic replicas,[20, 21] and block copolymer systems.[9, 22-26] The existence of 3D porous structure makes the mass transportation superior than the 2D channels and more resistant to clogging, which facilitate their applications in catalysis,[27] separation,[28] energy-related devices,[29, 30] pharmaceutical sciences,[31-33] environmental applications,[34, 35] etc. Therefore, it is of great importance to fully understand the formation mechanisms and the structural relationship of these structures.

In nature, these bicontinuous cubic structures are originated from the biological membranes. The cubic membranes often generated by the folding of planar biological membranes formed by lipids, particularly, in cells in response to starvation or oxidative stress, viral infection, abnormal protein expression, etc.[36-38] Deng et al. reported cubic membrane

occurred in the absence of food and disappeared in the sufficient of food in *amoeba* mitochondria.[36] Zhan et al reported the chloroplast membranes of green alga *Zygnema* could fold into multilayer gyroid biological cubic membranes in the culture at the end of log phase of cell growth.[39] In addition, the cubic membranes also appear in autoimmune cell,[40] cancer cells,[41] virally infected cells[37] and muscle cells with phosphatase abnormal expression.[38]

In artificial synthesis, the bicontinuous structures are normally discovered between the lamellae and cylindrical phases in both the theoretical[42-44] and experimental synthesis-field diagrams[45] employing amphiphilic molecules. Therefore, they are closely related to the lamellar and cylindrical precursors.[46-49] Theoretical models of the structural transition between lamellar and bicontinuous cubic phase are generally based on the formation of stalks between apposed lipid bilayers.[50, 51] The structure and energy of the stalk have considered elastic energy, splay, saddle splay, tilt deformations of the membrane and hydration repulsion acting between the apposed membranes.[52-54] A few experimental attempts have been carried out to provide evidence for the stalk theory of membrane fusion by temperature or pressure jump, laser illumination, and thermal scans that initiate the transition between the lamellar and cubic phases.[46, 47, 55-66] Demurtas et al. observed the lamellar-to-bicontinuous transition by cryo-electron tomography.[65] A

transition state named ILAs had been found between interior phase and the outside vesicular structure. Moreover, by carefully adjusting the lipid composition and adding stabilizer F127, Tran et al. reported the direct observation of a lamellar-to-bicontinuous transition in nanoscale dispersions.[66] They proposed that the bicontinuous cubic phase originates from the center of a lamellar vesicle then propagates outward via the formation of ILAs and stalks. However, the soft nature of the lipid systems greatly limited the detailed structural study.

The structural change was also revealed in the mesoporous structures templated by the surfactant molecules. Gallis et al. reported that MCM-48 could be obtained by a phase transformation from heating MCM-41 sample before incompletely polymerized.[67] They found ethanol, produced by hydrolysis of TEOS, plays a crucial role in the transformation process. Landry et al. studied the transformation of MCM-41 to MCM-48 and proposed that the phase transformation between MCM-41 and MCM-48 happens in an epitaxial manner, without dissolution of the initially formed MCM-41. Moreover, they proposed two competing mechanisms, one involving longitudinal linkage of hexagonal pores (cylinder merging) and the other involving transverse linkage (cylinder branching). The kinetic product is the lamellar phase, while the cubic phase is thermodynamically favored.[68] Compared to the MCM-48 with bicontinuous gyroid surface structure, the bicontinuous diamond surface structure is very rare. Gao et

al. obtained the mesoporous AMS-10 material with bicontinuous diamond structure in a narrow region close to the 2D hexagonal phase using anionic surfactant with co-structure directing agent.[69] In a previous report, we found the bicontinuous gyroid and diamond structures show similar surfactant geometrical parameter and forms various intermediate intergrowth with the continuous increasing of the organic/inorganic interfacial curvature in the synthesis system of anionic surfactant templated mesoporous silicas.[70] However, the structural relationship of the bicontinuous structure is still unclear and the intermediates between lamellar and bicontinuous structures have not been directly revealed.

In the previous synthesis, we reported a macroporous silica scaffold with shifted double diamond (SDD) and shifted double primitive (SDP) structures employing the cooperative self-assembly of ABC triblock terpolymer poly(ethylene oxide)-*b*-polystyrene-*b*-(poly(tert-butyl acrylate) (PEO-*b*-PS-*b*-PtBA) as template in the mixture solution of tetrahedron furan (THF) and water.[71, 72] The pore size can be over one hundred nanometers due to the block copolymer template and the solvent that significantly swelled the unit cell size. This synthesis system provides the possibility to investigate the structural intermediates by electron microscopy. Herein, we report the observation of structural change between macroporous bicontinuous diamond scaffold and lamellar structure. A series of inorganic intermediate phases have been obtained and

solidified by co-assembly of PEO-*b*-PS-*b*-PtBA and TEOS as silica source in a mixture of common solvent THF and the selective solvent HCl aqueous solution. Thanks to the stable silica frameworks, the macroporous silica scaffolds were characterized by small angle X-ray scattering (SAXS), scanning electron microscopy (SEM) and transmission electron microscopy (TEM) analysis in detail.

## 2. Methods:

### 2.1. Materials.

Monomethoxy poly(ethylene oxide) (PEO with molecular weight of 5000 g/mol) was purchased from Aldrich. methylene chloride (DCM), *N*, *N*-dimethylformamide (DMF) (>99 %) and *tert*-Butyl acrylate (*t*-BA) were purchased from J&K. *N*, *N*, *N'*, *N'*, *N*'-pentamethyldiethylenetriamine (PMDETA), hydrochloric acid (HCl, 36%), methyl alcohol (>99 %), Cuprous bromide (CuBr, 97 %), styrene, anhydrous ether (>99 %), THF (>99 %) and TEOS were purchased from Sinopharm Chemical Reagent Corp. Deionized water (Milli-Q, 18.2 MΩ·cm) were used in all experiments. The polymerization inhibitor of styrene and *t*-BA were removed through an Al<sub>2</sub>O<sub>3</sub> column.

### 2.2. Synthesis of PEO-Br.

The PEO-Br was introduced through the esterification of the hydroxyl in PEO-OH with 2-Bromoisobutyryl bromide in DCM. In detail, Dry PEO-OH (10 g, 2.0 mmol) was dissolved in dry DCM (50 mL). Then,

triethylamine (0.6 g, 6.0 mmol) and 2-Bromoisobutyrate bromide (6.9 g, 30 mmol) dissolved in DCM (25 mL) were added dropwise to the mixture for 30 min at 0 °C (ice-water bath). Finally, the mixture was stirred overnight at room temperature and then filtrated to obtain a homogeneous solution. The homogeneous solution was concentrated by evaporation. Subsequently, the concentrated solution was poured to 500 ml of cold ether to precipitate the PEO-Br, which was collected by filtration and dried under vacuum at room temperature.

### **2.3. Synthesis of $\text{PEO}_{113}\text{-}b\text{-}\text{PS}_{156}\text{-Br}$ .**

$\text{PEO}_{113}\text{-}b\text{-}\text{PS}_{156}\text{-Br}$  diblock copolymer was prepared via atom transfer radical polymerization (ATRP) technique of styrene at 110 °C, PEO-Br as the macroinitiator and CuBr/PMDETA as the catalyst system. Typically, a 250 mL Schlenk flask containing 4.0 g PEO-Br (0.80 mmol), 0.47 mL of PMDETA (2.26 mmol), and 50.0 g of styrene (0.29 mol) was mixed and then sealed with a rubber stopper. After the mixture became clear under stirring, 0.18 g CuBr (0.80 mmol) was added to the mixture. Finally, more than three freeze-pump-thaw cycles were used to completely degas the reaction system and sealed under vacuum. The Schlenk flask was then placed in an oil bath of 110 °C for about 6 h. After the mixture cooled to room temperature, the catalyst in the mixture was removed by exposing filtration through an  $\text{Al}_2\text{O}_3$  methylene chloride column using as eluent after the polymerization was terminated by exposing the reaction mixture to air.

The homogeneous solution was concentrated by evaporation. Subsequently, the concentrated solution was poured to 500 ml of cold ether to precipitate the PEO<sub>113</sub>-*b*-PS<sub>156</sub>-Br diblock copolymer, which was collected by filtration and dried under vacuum at room temperature.

#### **2.4. Synthesis of Template.**

PEO<sub>113</sub>-*b*-PS<sub>156</sub>-*b*-PtBA<sub>63</sub> was synthesized by ATRP of *t*-BA at 70 °C using PEO<sub>113</sub>-*b*-PS<sub>156</sub>-Br as the initiator, and CuBr/PMDETA as the catalyst system. In detail, 10.0 g PEO<sub>113</sub>-*b*-PS<sub>156</sub>-Br (0.76 mmol), 0.47 mL of PMDETA (2.28 mmol), 50.0 mL of *t*-BA and 25.0 ml DMF were added into a 250 mL Schlenk flask and then sealed with a rubber stopper. After the solution became clear with stirring, 0.109 g of CuBr (0.76 mmol) was added into the solutions. Finally, more than three freeze-pump-thaw cycles were used to completely degas the reaction system and sealed under vacuum. The Schlenk flask was then moved to oil bath of 70 °C to allow the polymerization to occur. The reaction time was controlled at 6 h. After the reaction, just like the synthesis of PEO<sub>113</sub>-*b*-PS<sub>156</sub>-Br, the mixtures were cooled to room temperature, the catalyst was removed, and the polymer was finally obtained by precipitation using cold methanol (500 mL).

#### **2.5. Synthesis of macroporous silica scaffolds.**

Three types of silica scaffolds were synthesized with template: THF: HCl (x M): TEOS = 1: 100: 20: 8, where x = 3, 6 and 12. In a typical synthesis, 0.1 g template was added into a 10 g THF solution of the

template and stirred for 2 h. Then, 0.8 g of TEOS was added into the solution. The mixed solution was stirred for another 2 h. Finally, the solution was evaporated at 15°C to remove solvent. The silica/template composite was washed with water three times and finally freeze-dried. The as-made sample was then calcined at 550 °C in air for 6 h to remove the template.

## 2.6. Characterizations.

The molecular weights and polydispersity index (PDI) were determined by HLC-8320GPC (TOSOH Corp.) gel permeation chromatography (GPC) apparatus, DMF was used as the eluent at a flow rate of 10-2000 μL/min. The nuclear magnetic resonance (NMR) spectra were measured by a Varian Mercury Plus 400 MHz NMR spectrometer, deuterated chloroform as solvent and tetramethylsilane (TMS) as the internal reference. The SAXS patterns were obtained by synchrotron radiation at beamline BL16B1 in Shanghai Synchrotron Radiation Facility (SSRF). SEM images of the sample were obtained by a JEOL JSM-7800F Prime at a low accelerating voltage of 1 kV with a specimen bias of -5 kV (point resolution of 0.7 nm). TEM observations were performed using a JEOL JEM-2100 microscope, which was equipped with a LaB<sub>6</sub> gun operated at 200 kV (Cs = 1.0 mm, point resolution of 2.3 Å). The TEM Images were obtained using a TENGRA CCD camera (2304×2304 pixels with a 2:1 fiber-optical taper and an effective pixel size of 18 μm<sup>2</sup>).

### 3. Results and Discussions

#### 3.1. Properties of the triblock terpolymer and the synthesis of the material.

The macroporous silica scaffold was prepared by the cooperative organization of the amphiphilic ABC triblock terpolymer PEO<sub>113</sub>-*b*-PS<sub>156</sub>-*b*-PtBA<sub>63</sub> as template and TEOS as silicon source. The template molecule was synthesized by ATRP with a total molar mass of 30.1 kg/mol and a polydispersity index of 1.52. In detail, the template had volume fractions of 14.6 %, 51.8 % and 33.6 % for the PEO, PS and PtBA blocks (see Figure S1, Figure S2 and Table S1 in the Supporting Information), respectively. Although the volume fraction of hydrophilic segment PEO (14.6 %) exceeded the range of 4-14 vol %, which is normally considered unsuitable for the formation of bicontinuous structures in the synthesis-field diagram.[73] However, the volume fraction in our system can be adjusted by the addition of solvents, which lead to the formation of the bicontinuous structure. The Flory-Huggins interaction parameters for polymer were calculated as  $\chi_{AS}N \approx 5.85$ ,  $\chi_{AO}N \approx 54.8$  and  $\chi_{SO}N \approx 41.2$ ,  $\chi N = \sum N \times \frac{V_{ref} \times (\delta_1 - \delta_2)^2}{RT}$  where  $V_{ref}$  is the segment reference volume ( $V_{ref} = 100$  cm<sup>3</sup>/mol), and  $\delta_i$  is the Hildebrand solubility parameter for polymer  $i$  ( $\delta_A = 18.5$  (J/cm<sup>3</sup>)<sup>1/2</sup>,  $\delta_S = 19.3$  (J/cm<sup>3</sup>)<sup>1/2</sup>, and  $\delta_O = 21.2$  (J/cm<sup>3</sup>)<sup>1/2</sup>). In the synthesis system, the triblock terpolymer was dissolved in the common solvent THF due to the similar solubility parameters of THF ( $\delta = 18.6$

$[J/cm^3]^{1/2}$ ) and triblock terpolymer. However, the microphase separation occurred when adding the HCl aqueous solution due to the  $H_2O$  is the selective solvent ( $\delta = 47.8 [J/cm^3]^{1/2}$ ). The hydrophobic blocks PtBA and PS are present in the THF-rich phase and the PEO is present in the  $H_2O$ -rich phase. TEOS would be hydrolyzed and condensed in the  $H_2O$ -rich phase through the co-interaction of hydrogen bonding between ethylene oxide and silanol and the electrostatic interaction between  $EO_{m-y}[(EO) \cdot H_3O^+]_y$  and  $[yCl^- \cdot Si(OH)^{2+}]$ .<sup>[74]</sup> Pure inorganic silica scaffolds can be obtained by removing the template molecules by calcination at 550°C.

### 3.2. Structural change with different HCl concentration.

Three types of macroporous silica scaffolds were synthesized with template: THF: HCl (x M): TEOS = 1: 100: 20: 8. The samples were denoted as macroporous silica 1 to 3 (MS-1, MS-2 and MS-3) synthesized with  $x = 3, 6$  and 12, respectively.

Figure 1 shows the SAXS patterns of the samples. As shown in Figure 1a, the MS-1 represents several reflections, indicating highly ordered structure. The main structure is later determined to be the macroporous bicontinuous double diamond (DD) surface structure. However, the double diamond frameworks are shifted to adhere with each other, forming a low-symmetry SDD structure with space group  $I4_1/AMD$ . The unit-cell parameters are  $a_{SDD} \approx 110$  nm and  $c_{SDD} \approx 156$  nm  $\approx \sqrt{2}a_{SDD}$ . The SAXS pattern of MS-2 is shown in Figure 1b, which the Bragg positions

of the 101 and 200 reflections become weaker comparing with MS-1. As shown in Figure 1c, the MS-3 has no obvious reflection, indicating the disordered structure.

Figure 2 shows the SEM images of MS-1. The low-magnification SEM image of the sample is shown in Figure 2a, revealing the single crystal feature with several tens of micron in size. Several growth steps can be clearly observed. High magnification SEM image (Figure 2b) shows two sets of continuous silica networks following the tetrahedral arrangement, revealing the diamond-surface morphology. Both networks are hollow with thin silica wall. Moreover, the two sets of networks are closely adhered to each other, forming SDD structure. The wide edge of the macropore is ~90 nm. It is worthy to note that, the cubic DD structure was initially obtained.[71] However, the two networks of DD can be freely moved when solvents were removed. The shift is along one of the original  $<100>_{\text{cubic}}$  axis of the DD structure due to the maximize of the contact area of the PS and PtBA segments with hydrophobic interaction.[71] Therefore, a tetragonal SDD structure with space group  $I4_1/\text{amd}$  can be formed (Figure 2c and 2d).

When the concentration of HCl was changed to 6 M, bicontinuous DD surface structure with several intermediates between lamellar and bicontinuous structures had been obtained. As shown in Figure 3a, the normal cubic DD structure without shift can be seen at the bottom left of

the SEM image. However, the wide edge of the macropore is about 200 nm and the smallest entrance of the hollow tube (in the middle of the nodes) is 100-150 nm. It can be seen the diameter of the hollow tube is much larger than that of MS-1. As enclosed in the white region in Figure 3a, a porous lamellar structure can be observed, which consists of a whole surface with open necks toward perpendicular direction. The cross-sectional view of the porous lamellar is presented in Figure 3c. It can be seen the layers are not isolated and they are interconnected with each other by the hollow necks, which are known as stalks (red arrows).[47, 50, 52] Therefore, the arms of DD structure may be originated from the stalks, as indicated by red and black circles in the enlarged SEM image (Figure 3b). According to the SEM images, an epitaxial relationship is confirmed, which the {111} plane of DD structure is parallel to the lamellar structures. This is in agree with the structural transition between lamellar and diamond surfaces in liquid crystal systems.[75] In Figure 3d, a transition center has been discovered, which includes a disordered hyperbolic surface-type core surrounded by lamellar structures. It can be seen that the lamellar structures directly connected to the core part by spreading the hyperbolic surface out of the transition center. Each layer of the lamellar connect to one set of surface of the DD structure. At the boundary of the lamellar and the bicontinuous part, some stalks and holes can be also observed as indicated by red arrows.

By adjusting the concentration of HCl to 12 M, an intermediate

structure much different from above was obtained. Figure 4a reveals the overall information of the sample MS-3. Porous lamellar structure is the main phase and some regions contain transition centers as indicated by blue circles. Figure 4b shows one transition center, which is surrounded by clear lamellar structures as marked by blue arrows. These lamellar structures are closely attached with each other, which may due to the solvent evaporation that caused the collapse. It could be observed that the bicontinuous structures are originated from the center and spread out gradually. These lamellar structures have different orientations and it is difficult to confirm the epitaxial relationship because no ordered DD structure have been obtained. However, ILAs (red arrow) have been found between lamellar layers. These intermediate structures resemble the intermediate phases of layered membranes transforming to cubic membranes in certain stimulations in cells.[36-38] Figure 4c and 4d show the TEM images of bicontinuous nucleation. The transition centers surrounded by lamellar silica structures (blue arrows) can be also clarified. The junction of the lamellar structures and the bicontinuous structure can be clearly seen (black arrows), showing the direct connection of the hyperbolic surface and the lamellar plane. It is also worthy to note that the lamellar structures become curved to equalize the curvature change over the structural transition, resulting in the formation of the bicontinuous cubic structures with high symmetry. This result is consistent with the result of SEM

observation. To demonstrate the universality of the centers, a similar series of morphologies is provided in the Supplementary Information Figure S3, all showing the similar relationship. The transition centers act as seeds for the growth of bicontinuous structures.

### **3.3. Speculation of the Formation of the Macroporous Structures.**

In nature, the bicontinuous cubic membranes are always originated from biological membranes transformation. In order to understanding the relevant mechanism, the transformations between lamellar and bicontinuous structures in lipid system were extensively examined. Of note, the membrane fusion models between apposed lipid bilayers all rely on the formation of transient lipid contacts known as stalks, which subsequently break through to form the inverse bicontinuous cubic phases.[47, 51, 76, 77] Siegel et al predicted that the relative free energy of intermediates in the transitions between lamellar inverted hexagonal ( $H_{II}$ ), and inverted cubic ( $Q_{II}$ ) phases by using a model of the energetics of lipid assemblies in the system of water/dioleoylphosphatidylethanolamine (DOPE).[50] The model proposed by Siegel et al[78] was previously used to generate the modified stalk theory of membrane fusion. The modified stalk theory proposes that the lowest energy structures to form between apposed membranes are the stalk and the transmonolayer contact (TMC), respectively. Kozlovsky et al predicted expansion of the fusion stalk into an hemifusion diaphragm for lipids characterized by a sufficiently negative

spontaneous curvature. Radial expansion of the stalk is found to be more favorable energetically than linear expansion in all practically important cases. They showed that the elastic stresses of tilt and splay of the hydrocarbon chains developed in the region of the diaphragm rim generate the lateral tension. This tension can be sufficiently large to result in formation of a fusion pore expanding along the rim and leading to completion of the fusion reaction. In contrast to recent models suggesting direct transition from a stalk to a pore, the results of their analysis indicate the possibility of hemifusion diaphragm expansion followed by fusion pore formation.[51] The intermediates observed by SEM clearly prove the phase transition through ILAs and the existence of fusion pore, which is consistent with the previous research.[47, 56, 61, 65, 66] However, we found the size of the fusion pore would change throughout the transition in real experiment. Moreover, previous reports showed the transition through concentric bilayers of an “onion-like” multi membrane vesicle. Toward the center of the vesicle, a more disordered structure is observed.[47, 66] However, in our system, no “onion-like” multi membrane vesicle have been observed. An epitaxial relationship has been confirmed, which the {111} plane of DD structure is parallel to the plane of porous lamellar structures, which shows the same structural relationship with the previous reports.[75] Specially, one of the four arms in one node of DD structure is originated from ILAs. It is worthy to note that, transformation centers are

often observed in our system, which may be formed by perturbation of the synthesis system that act as the nucleus of the structural formation.

Herein, the block polymer was used as template and the formation of macroporous structures is both thermodynamically and kinetically controlled. The polymer chain moves slower during the transition and the stable silica framework was formed by the cooperative self-assembly of the inorganic precursor with ethylene oxide by hydrogen bonding and the electrostatic interaction between  $\text{EO}_{m-y}[(\text{EO})\cdot\text{H}_3\text{O}^+]_y$  and  $[\text{yCl}^-\cdot\text{Si}^-\text{OH}^{2+}]$  to fix the intermediate phases. The structure is determined by the packing parameter  $p = V/a_0l$ ,  $V$  is the volume of the hydrophobic segment,  $a_0$  is the contact area of the head group, and  $l$  is the length of the hydrophobic segment.[79] Thus, adding another amphiphilic molecule is not needed comparing with previous studies. Moreover, the self-assembly of block polymer in dual solvent can obtain advanced length scale for observation comparing with lipid system. It is worthy to note that, the DD structure is difficult to be formed because it is a thermodynamically unfavored structure. This structure was only discovered in very narrow window compared to the normally observed bicontinuous gyroid structure.[71, 80, 81] In our system, the synthesis was performed with solvent evaporation. The formation of the final structure was both thermodynamically and kinetically controlled. Therefore, the DD or SDD structure can be formed in the synthesis. Of note, it has been well established that electrostatic

interactions due to surface charges of lipid membranes play various important roles in the structures and phase stabilities of the bicontinuous phase.[82-85] We believe that with the increase of HCl, more H<sup>+</sup> present in the PEO-rich phase by hydrogen bonding, the repulsive force in the PEO end increases. Therefore, the packing parameter changed from  $p > 1$  to  $p = 1$  in the reverse micelle configuration, leading to DD structure with larger unit cell size with smaller organic/inorganic interfacial curvature and to form the lamellar structure.

Based on the above discussions, we propose a 2-step mechanism for the transition from lamellar to DD macroporous structures. In the first step, stalks are formed across the H<sub>2</sub>O-rich phase. This can be justified by the asymmetry in the volume fractions. These stalks expand into pores through H<sub>2</sub>O-rich phases, leading to hexagonally perforated layers (HPLs). In the second step, tubes are formed between the HPLs. There are two possibilities: If tubes only connect adjacent HPLs, the result would be a SD structure. If tubes pass through the pores of HPLs, the result would be a DD structure. From the geometrical consideration, the DD structure can be formed only when the tubes pass through the pores of HPLs. The double networks can be then formed by connecting every other layers of lamellar structure. This means that the pores in HPLs form and expand very rapidly and HPLs can become planar hexagonal networks before the tubes are formed (Figure 5).

## **4. Conclusions**

In summary, the inorganic intermediates from lamellar-to-bicontinuous structural transition have been observed by changing the concentration of HCl in the synthesis system of block copolymer and inorganic source. Our results show that the existence of the transition center may act as a seed for the growth of the bicontinuous structures. The stalks or ILAs also play key role in the transition process. Moreover, we speculate that a possible kinetic pathway during the lamellar-to-bicontinuous phase transition. We believe the system of amphiphilic block copolymer with inorganic source is a good choice for the structural study of these cubic phases and our results may bring new insights to the formation of these hyperbolic surfaces in biological systems. Moreover, the study of structural transformation helps us develop new types of porous materials with remarkable applications.

## **Acknowledgement**

This work was supported by the National Natural Science Foundation of China (21922304, L.H.), Natural Science Foundation of Shanghai (18ZR1442400, L.H.) and Individual Research Grant from Deutsche Forschungsgemeinschaft within the project “Defects in Triply Periodic Minimal Surfaces” (398759432, H.C.). We thank the Shanghai Synchrotron Radiation Facility (SSRF) for providing access to the BL16B1 beamline for collecting synchrotron SAXS data.

## References

- [1] K.C.W. Wu, X. Jiang, Y. Yamauchi, *Journal of Materials Chemistry*, 21 (2011) 8934-8939, [https://doi.org/10.1039/C1JM10548E..](https://doi.org/10.1039/C1JM10548E)
- [2] W.H. Kim, S.Y. Choi, Y.M. Jeon, S. Lee, S.H. Kim, *ACS Applied Materials & Interfaces*, 6 (2014) 11484-11492, <https://doi.org/10.1021/am502137d>.
- [3] Y. Guo, J. Tang, J. Henzie, B. Jiang, H. Qian, Z. Wang, H. Tan, Y. Bando, Y. Yamauchi, *Materials Horizons*, 4 (2017) 1171-1177, <https://doi.org/10.1039/C7MH00586E>.
- [4] X. Xu, A.E. Allah, C. Wang, H. Tan, A.A. Farghali, M.H. Khedr, V. Malgras, T. Yang, Y. Yamauchi, *Chemical Engineering Journal*, 362 (2019) 887-896, <https://doi.org/10.1016/j.cej.2019.01.098>.
- [5] Y. Wan, D. Zhao, *Chemical Reviews*, 107 (2007) 2821-2860, <https://doi.org/10.1021/cr068020s>
- [6] J.-L. Blin, A. Léonard, Z.-Y. Yuan, L. Gigot, A. Vantomme, A.K. Cheetham, B.-L. Su, *Angewandte Chemie*, 115 (2003) 2978-2981, [doi.org/10.1002/ange.200250816](https://doi.org/10.1002/ange.200250816).
- [7] K. Shen, L. Zhang, X. Chen, L. Liu, D. Zhang, Y. Han, J. Chen, J. Long, R. Luque, Y. Li, B. Chen, *Science*, 359 (2018) 206, doi: [10.1126/science.aaq3403](https://doi.org/10.1126/science.aaq3403).
- [8] S.W. Robbins, P.A. Beaucage, H. Sai, K.W. Tan, J.G. Werner, J.P. Sethna, F.J. DiSalvo, S.M. Gruner, R.B. Van Dover, U. Wiesner, *Science Advances*, 2 (2016) e1501119, DOI: [10.1126/sciadv.1501119](https://doi.org/10.1126/sciadv.1501119).
- [9] M. Stefk, S. Guldin, S. Vignolini, U. Wiesner, U. Steiner, *Chemical Society Reviews*, 44 (2015) 5076-5091, <https://doi.org/10.1039/C4CS00517A>.
- [10] P. Brandt, G. Pappas, *J. Biophysic. and Biochem. Cytol*, 6 (1959) 91, doi: [10.1083/jcb.6.1.91](https://doi.org/10.1083/jcb.6.1.91).
- [11] Z.A. Almsherqi, S.D. Kohlwein, Y. Deng, *The Journal of Cell Biology*, 173 (2006) 839, doi:[10.1083/jcb.200603055](https://doi.org/10.1083/jcb.200603055).
- [12] Y. Deng, M. Mieczkowski, *Protoplasma*, 203 (1998) 16-25, doi:[10.1007/BF01280583](https://doi.org/10.1007/BF01280583).
- [13] J.W. Galusha, L.R. Richey, J.S. Gardner, J.N. Cha, M.H. Bartl, *Physical Review E*, 77 (2008) 050904, doi:[10.1103/PhysRevE.77.050904](https://doi.org/10.1103/PhysRevE.77.050904).
- [14] B.D. Wilts, H.L. Leertouwer, D.G. Stavenga, *Journal of The Royal Society Interface*, 6 (2009) S185-S192, doi:[10.1098/rsif.2008.0299.focus](https://doi.org/10.1098/rsif.2008.0299.focus)
- [15] K. Michelsen, D.G. Stavenga, *Journal of The Royal Society Interface*, 5 (2008) 85-94, doi:[10.1098/rsif.2007.1065](https://doi.org/10.1098/rsif.2007.1065).
- [16] R. Holyst, *Nature materials*, 4 (2005) 510-511, <https://doi.org/10.1038/nmat1419>.
- [17] J. Charvolin, J. Sadoc, *Journal De Physique*, 48 (1987) 1559-1569, doi: [10.1051/jphys:019870048090155900](https://doi.org/10.1051/jphys:019870048090155900).
- [18] J.F. Sadoc, J. Charvolin, *Acta Crystallographica Section A*, 45 (1989) 10-20, doi: [10.1107/S0108767388008438](https://doi.org/10.1107/S0108767388008438).
- [19] P. Barois, S.T. Hyde, B.W. Ninham, T. Dowling, *Langmuir*, 6 (1990) 1136-1140, doi: <https://doi.org/10.1021/la00096a019>.
- [20] C.T. Kresge, M.E. Leonowicz, W.J. Roth, J.C. Vartuli, J.S. Beck, *Nature*, 359 (1992) 710-712, doi: <https://doi.org/10.1038/359710a0>
- [21] Y. Wan, D. Zhao, 107 (2007) 2821-2860, <https://doi.org/10.1021/cr068020s>
- [22] M.C. Orilall, U. Wiesner, *Chemical Society Reviews*, 40 (2011) 520-535, <https://doi.org/10.1039/C0CS00034E>.
- [23] E.L. Thomas, D.M. Anderson, C.S. Henkee, D. Hoffman, *Nature*, 334 (1988) 598-601, <https://doi.org/10.1038/334598a0>.
- [24] Y. Mai, A. Eisenberg, 41 (2012) 5969-5985, <https://doi.org/10.1039/C2CS35115C>

- [25] D.A. Hajduk, P.E. Harper, S.M. Gruner, C.C. Honeker, G. Kim, E.L. Thomas, L.J. Macromolecules, 27 (1994) 4063-4075, <https://doi.org/10.1021/ma00093a00>.
- [26] E.W. Cochran, C.J. Garciacervera, G.H. Fredrickson, Macromolecules, 39 (2006) 2449-2451, <https://doi.org/10.1021/ma0527707>.
- [27] M.S. Morey, A. Davidson, G.D. Stucky, Silica-Based, Journal of Porous Materials, 5 (1998) 195-204, <https://doi.org/10.1023/A:1009626103498>.
- [28] N. Sreedhar, N. Thomas, O. Al-Ketan, R. Rowshan, H.H. Hernandez, R.K.A. Al-Rub, H.A. Arafat, Mass Journal of Membrane Science, 561 (2018) 89-98, <https://doi.org/10.1016/j.memsci.2018.05.028>.
- [29] L. Zhang, S. Feih, S. Daynes, S. Chang, M.Y. Wang, J. Wei, W.F. Lu, Additive Manufacturing, 23 (2018) 505-515, <https://doi.org/10.1016/j.addma.2018.08.007>.
- [30] E.J. Crossland, M. Kamperman, M. Nedelcu, C. Ducati, U. Wiesner, D.-M. Smilgies, G.E. Toombes, M.A. Hillmyer, S. Ludwigs, U. Steiner, Nano letters, 9 (2009) 2807-2812, <https://doi.org/10.1021/nl803174p>.
- [31] M. Vallet-Regi, A. Ramila, R. Del Real, J. Pérez-Pariente, Chemistry of Materials, 13 (2001) 308-311, <https://doi.org/10.1021/cm0011559>.
- [32] J.C. Shah, Y. Sadhale, D.M. Chilukuri, Advanced drug delivery reviews, 47 (2001) 229-250, [https://doi.org/10.1016/S0169-409X\(01\)00108-9](https://doi.org/10.1016/S0169-409X(01)00108-9).
- [33] C.J. Drummond, C. Fong, Current opinion in colloid & interface science, 4 (1999) 449-456, [https://doi.org/10.1016/S1359-0294\(00\)00020-0](https://doi.org/10.1016/S1359-0294(00)00020-0).
- [34] M. Morey, A. Davidson, G. Stucky, Journal of Porous Materials, 5 (1998) 195-204, <https://doi.org/10.1023/A:1009626103498>.
- [35] S. Lou, X. Guo, T. Fan, D. Zhang, Energy & Environmental Science, 5 (2012) 9195-9216, <https://doi.org/10.1039/C2EE03595B>.
- [36] Y. Deng, M. Mieczkowski, Protoplasma, 203 (1998) 16-25, <https://doi.org/10.1007/BF01280583>.
- [37] Y. Deng, Z.A. Almsherqi, M.M. Ng, S.D. Kohlwein, Trends in cell biology, 20 (2010) 371-379, <https://doi.org/10.1016/j.tcb.2010.04.001>.
- [38] L. Amoasii, K. Hnia, G. Chicanne, A. Brech, B.S. Cowling, M.M. Müller, Y. Schwab, P. Koebel, A. Ferry, B. Payrastre, Journal of cell science, 126 (2013) 1806-1819, doi: 10.1242/jcs.118505.
- [39] T. Zhan, W. Lv, Y. Deng, Protoplasma, 254 (2017) 1923-1930, <https://doi.org/10.1007/s00709-017-1083-2>.
- [40] A. Mak, Z.A. Almsherqi, Y.W. Lai, A.A.C. Cheak, Y. Deng, International journal of rheumatic diseases, 16 (2013) 692-697, <https://doi.org/10.1111/1756-185X.12195>.
- [41] Z. Schaff, K. Lapis, P. Grimley, International journal of cancer, 18 (1976) 697-702, <https://doi.org/10.1002/ijc.2910180519>.
- [42] M.W. Matsen, M. Schick, Stable and unstable phases of a diblock copolymer melt, Physical Review Letters, 72 (1994) 2660.
- [43] M. Matsen, F.S. Bates, Macromolecules, 29 (1996) 1091-1098, <https://doi.org/10.1021/ma951138i>.
- [44] T. Honda, T. Kawakatsu, Macromolecules, 39 (2006) 2340-2349, doi:10.1021/ma052075z.
- [45] A.K. Khandpur, S. Foerster, F.S. Bates, I.W. Hamley, A.J. Ryan, W. Bras, K. Almdal, K. Mortensen, Macromolecules, 28 (1995) 8796-8806, <https://doi.org/10.1021/ma00130a012>.
- [46] B. Angelov, A. Angelova, U. Vainio, V.M. Garamus, S. Lesieur, R. Willumeit, P. Couvreur, Langmuir, 25 (2009) 3734-3742, doi:10.1021/la804225j.
- [47] C.E. Conn, O. Ces, X. Mulet, S. Finet, R. Winter, J.M. Seddon, R.H. Templer, Physical Review Letters, 96 (2006) 108102, doi:10.1103/PhysRevLett.96.108102.

- [48] M.F. Schulz, F.S. Bates, K. Almdal, K. Mortensen, *Physical review letters*, 73 (1994) 86, doi: 10.1103/PhysRevLett.73.86.
- [49] M.W. Matsen, *Physical review letters*, 80 (1998) 4470, <https://doi.org/10.1103/PhysRevLett.80.4470>.
- [50] D.P. Siegel, *Biophysical Journal*, 76 (1999) 291-313, [https://doi.org/10.1016/S0006-3495\(99\)77197-3](https://doi.org/10.1016/S0006-3495(99)77197-3).
- [51] Y. Kozlovsky, L.V. Chernomordik, M.M. Kozlov, *Biophysical Journal*, 83 (2002) 2634-2651, [https://doi.org/10.1016/S0006-3495\(02\)75274-0](https://doi.org/10.1016/S0006-3495(02)75274-0).
- [52] Y. Kozlovsky, A. Efrat, D.A. Siegel, M.M. Kozlov, *Biophysical Journal*, 87 (2004) 2508-2521, <https://doi.org/10.1529/biophysj.103.038075>.
- [53] D.P. Siegel, M.M. Kozlov, *Biophysical Journal*, 87 (2004) 366-374, <https://doi.org/10.1529/biophysj.104.040782>.
- [54] Y. Kozlovsky, M.M. Kozlov, *Biophysical Journal*, 82 (2002) 882-895, <https://doi.org/10.1529/biophysj.103.038075>.
- [55] C.V. Kulkarni, T.-Y. Tang, A.M. Seddon, J.M. Seddon, O. Ces, R.H. Templer, *Soft Matter*, 6 (2010) 3191-3194, <https://doi.org/10.1039/C0SM00068J>.
- [56] X. Mulet, X. Gong, L.J. Waddington, C.J. Drummond, *ACS Nano*, 3 (2009) 2789-2797, doi:10.1021/nn900671u.
- [57] B. Angelov, A. Angelova, M. Ollivon, C. Bourgaux, A. Campitelli, *Journal of the American Chemical Society*, 125 (2003) 7188-7189, <https://doi.org/10.1021/ja034578v>.
- [58] B. Angelov, A. Angelova, V.M. Garamus, G. Lebas, S. Lesieur, M. Ollivon, S.S. Funari, R. Willumeit, P. Couvreur, *Journal of the American Chemical Society*, 129 (2007) 13474-13479, <https://doi.org/10.1021/ja072725+>.
- [59] Y.-D. Dong, A.J. Tilley, I. Larson, M.J. Lawrence, H. Amenitsch, M. Rappolt, T. Hanley, B.J. Boyd, *Langmuir*, 26 (2010) 9000-9010, <https://doi.org/10.1021/la904803c>.
- [60] B. Angelov, A. Angelova, S.K. Filippov, M. Drechsler, P. Štěpánek, S. Lesieur, *ACS Nano*, 8 (2014) 5216-5226, doi:10.1021/nn5012946.
- [61] B. Angelov, A. Angelova, V.M. Garamus, M. Drechsler, R. Willumeit, R. Mutafchieva, P. Štěpánek, S. Lesieur, *Langmuir*, 28 (2012) 16647-16655, doi:10.1021/la302721n.
- [62] B. Angelov, A. Angelova, R. Mutafchieva, S. Lesieur, U. Vainio, V.M. Garamus, G.V. Jensen, J.S. Pedersen, *Physical Chemistry Chemical Physics*, 13 (2011) 3073-3081, doi:10.1039/C0CP01029D.
- [63] M. Seddon John, M. Squires Adam, E. Conn Charlotte, O. Ces, J. Heron Andrew, X. Mulet, C. Shearman Gemma, H. Templer Richard, *Physical and Engineering Sciences*, 364 (2006) 2635-2655, doi:10.1098/rsta.2006.1844.
- [64] T.Y.D. Tang, N.J. Brooks, C. Jeworrek, O. Ces, N.J. Terrill, R. Winter, R.H. Templer, J.M. Seddon, *Langmuir*, 28 (2012) 13018-13024, doi:10.1021/la3025843.
- [65] D. Demurtas, P. Guichard, I. Martiel, R. Mezzenga, C. Hébert, L. Sagalowicz, *Nature Communications*, 6 (2015) 8915, doi:10.1038/ncomms9915.
- [66] N. Tran, J. Zhai, C.E. Conn, X. Mulet, L.J. Waddington, C.J. Drummond, *The Journal of Physical Chemistry Letters*, 9 (2018) 3397-3402, (doi:10.1021/acs.jpclett.8b01110).
- [67] K.W. Gallis, C.C. Landry, *Chemistry of Materials*, 9 (1997) 2035-2038, doi:10.1021/cm970482m.
- [68] C.C. Landry, S.H. Tolbert, K.W. Gallis, A. Monnier, G.D. Stucky, P. Norby, J.C. Hanson, *Chemistry of Materials*, 13 (2001) 1600-1608, doi:10.1021/cm000373z.
- [69] C. Gao, Y. Sakamoto, O. Terasaki, S. Che, *Chemistry-A European Journal*, 14 (2008) 11423-11428,

<https://doi.org/10.1002/chem.200800766>.

- [70] L. Han, K. Miyasaka, O. Terasaki, S. Che, *Journal of the American Chemical Society*, 133 (2011) 11524-11533, doi:10.1021/ja200683t.
- [71] L. Han, D. Xu, Y. Liu, T. Ohsuna, Y. Yao, C. Jiang, Y. Mai, Y. Cao, Y. Duan, S. Che, *Chemistry of Materials*, 26 (2014) 7020-7028, <https://doi.org/10.1021/cm5033139>.
- [72] W. Mao, X. Cao, Q. Sheng, L. Han, S. Che, *Angewandte Chemie*, 129 (2017) 10810-10815, <https://doi.org/10.1002/anie.201704639>.
- [73] T.S. Bailey, C.M. Hardy, T.H. Epps, F.S. Bates, *Macromolecules*, 35 (2002) 7007-7017, doi:10.1021/ma011716x.
- [74] D. Zhao, Q. Huo, J. Feng, B.F. Chmelka, G.D. Stucky, *Journal of the American Chemical Society*, 120 (1998) 6024-6036, <https://doi.org/10.1021/ja974025i>.
- [75] A.M. Squires, R.H. Templer, J.M. Seddon, J. Woenckhaus, R. Winter, S. Finet, N. Theyencheri, *Langmuir*, 18 (2002) 7384-7392, doi:10.1021/la0259555.
- [76] L.V. Chernomordik, M.M. Kozlov, *Annual Review of Biochemistry*, 72 (2003) 175-207, <https://doi.org/10.1146/annurev.biochem.72.121801.161504>.
- [77] D.P. Siegel, *Biophysical Journal*, 49 (1986) 1171-1183, doi: 10.1016/S0006-3495(86)83745-6.
- [78] D.P. Siegel, *Biophysical journal*, 65 (1993) 2124-2140, doi: 10.1016/S0006-3495(93)81256-6.
- [79] J.N. Israelachvili, D.J. Mitchell, B.W. Ninham, *Journal of the Chemical Society, Faraday Transactions 2: Molecular and Chemical Physics*, 72 (1976) 1525-1568, <https://doi.org/10.1039/F29767201525>.
- [80] C. Gao, Y. Sakamoto, K. Sakamoto, O. Terasaki, S. Che, *Angew Chem Int Ed Engl*, 45 (2006) 4295-4298, <https://doi.org/10.1002/anie.200504114>.
- [81] A.J. Meuler, M.A. Hillmyer, F.S. Bates, *Macromolecules*, 42 (2009) 7221-7250, doi: 10.1021/ma9009593.
- [82] T. Oka, T.-a. Tsuboi, T. Saiki, T. Takahashi, J.M. Alam, M. Yamazaki, *Langmuir*, 30 (2014) 8131-8140, <https://doi.org/10.1021/la5021719>.
- [83] T. Oka, T. Saiki, J.M. Alam, M. Yamazaki, *Langmuir*, 32 (2016) 1327-1337, <https://doi.org/10.1021/acs.langmuir.5b03785>.
- [84] T. Oka, M. Hasan, M.Z. Islam, M. Moniruzzaman, M. Yamazaki, *Langmuir*, 33 (2017) 12487-12496, <https://doi.org/10.1021/acs.langmuir.7b02512>.
- [85] Y. Okamoto, S.M. Masum, H. Miyazawa, M. Yamazaki, *Langmuir*, 24 (2008) 3400-3406, <https://doi.org/10.1021/la7036795>.

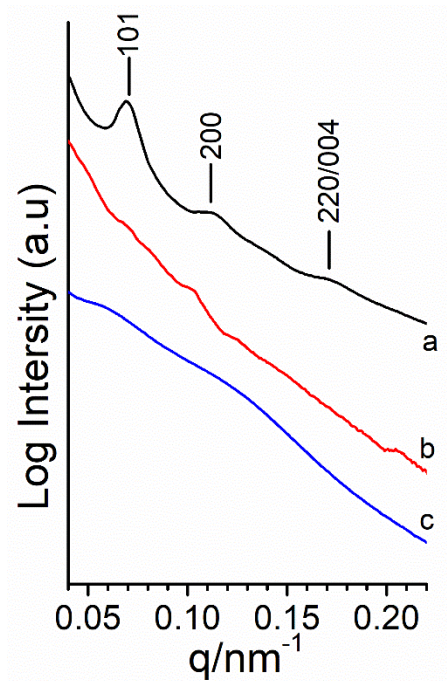


Figure 1. SAXS patterns of the calcined materials. (a) MS-1, (b) MS-2 and (c) MS-3.

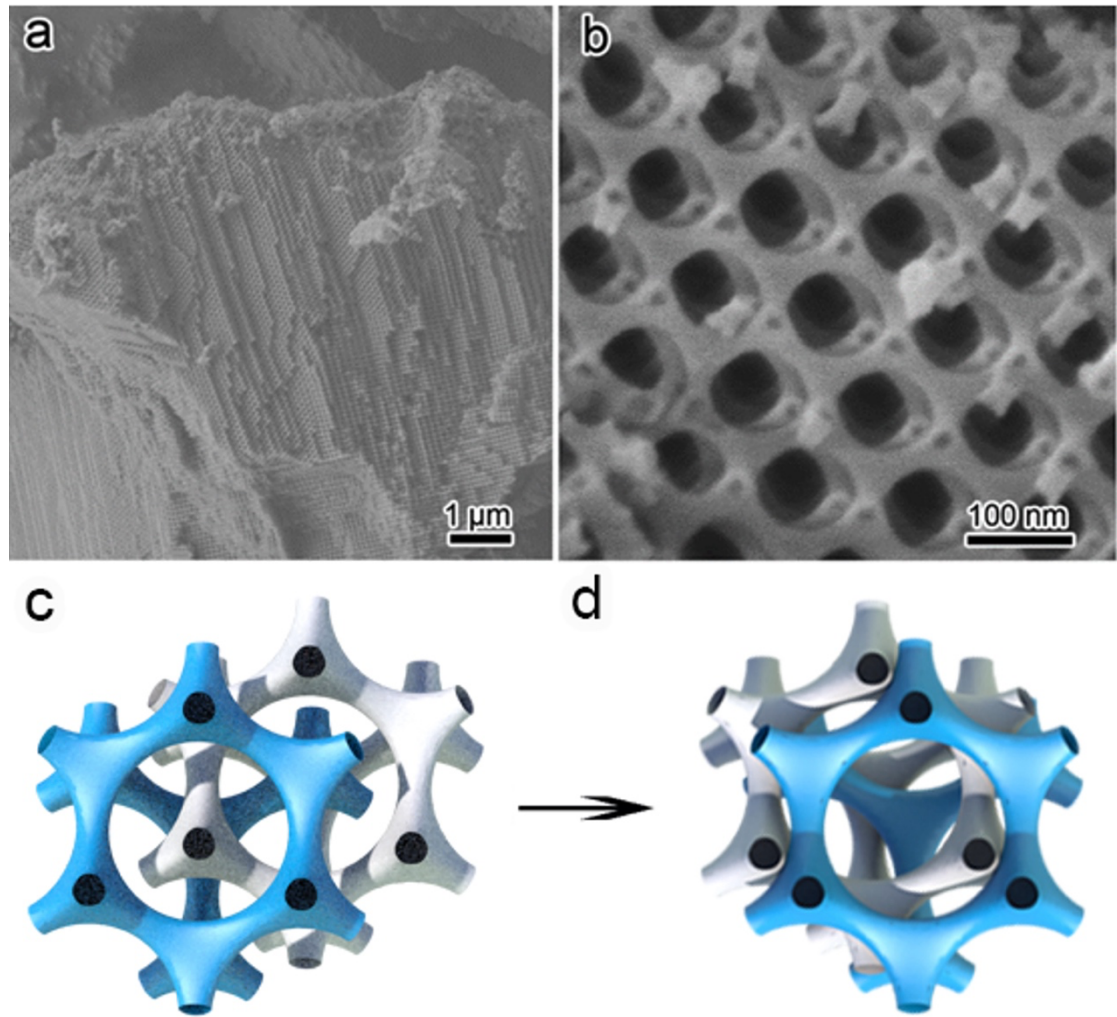


Figure 2. SEM images of MS-1. (a) Low-magnification and (b) high-magnification SEM image of MS-1. Structural models of DD (c) and SDD (d).

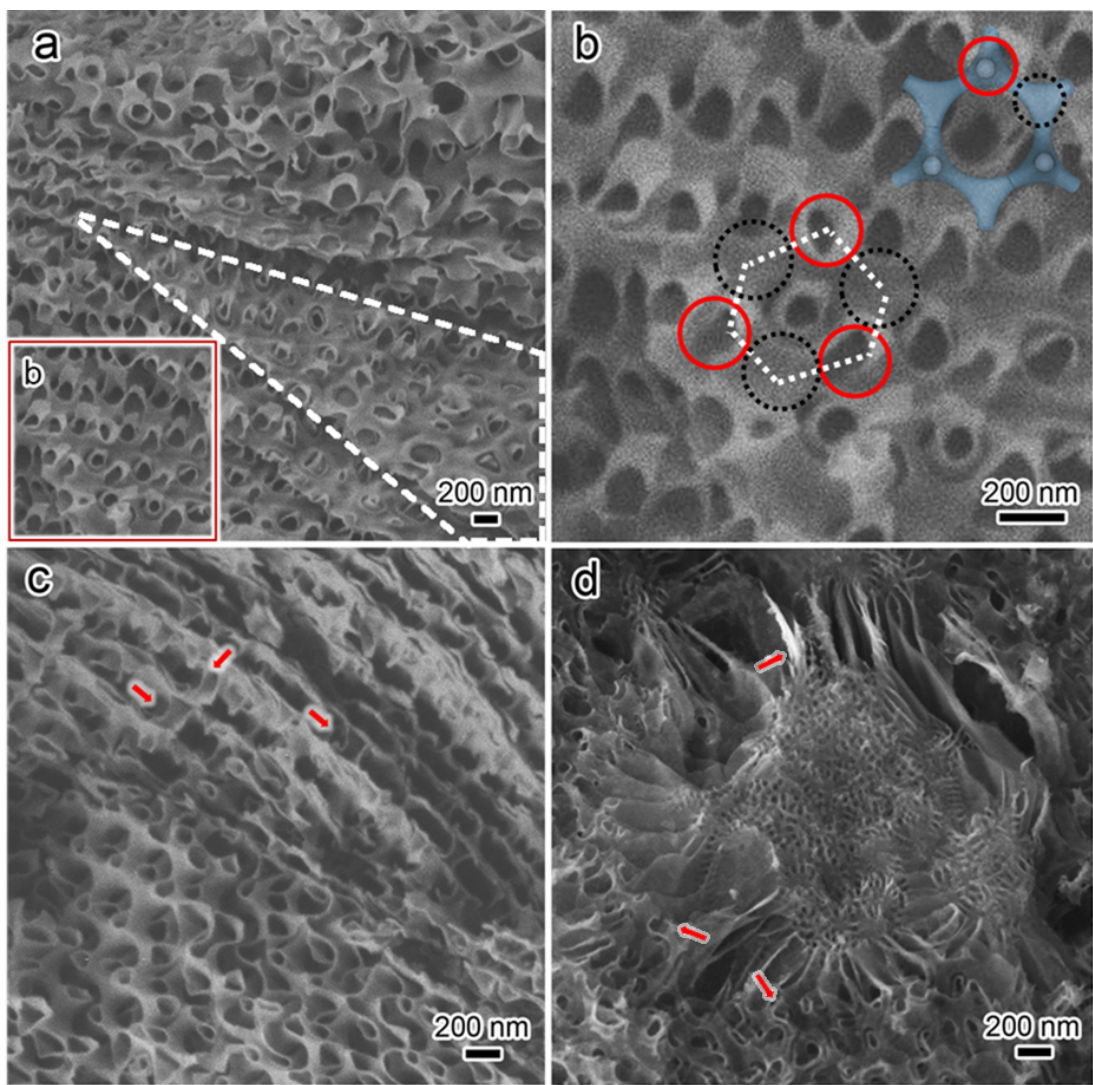


Figure 3. SEM images of MS-2. (a, b) SEM image of the intergrown structure of porous lamellar structure (top view) and DD. (c) SEM image of the intergrown structure of porous lamellar structure (side view) and SDD. (d) SEM image of a transition center.

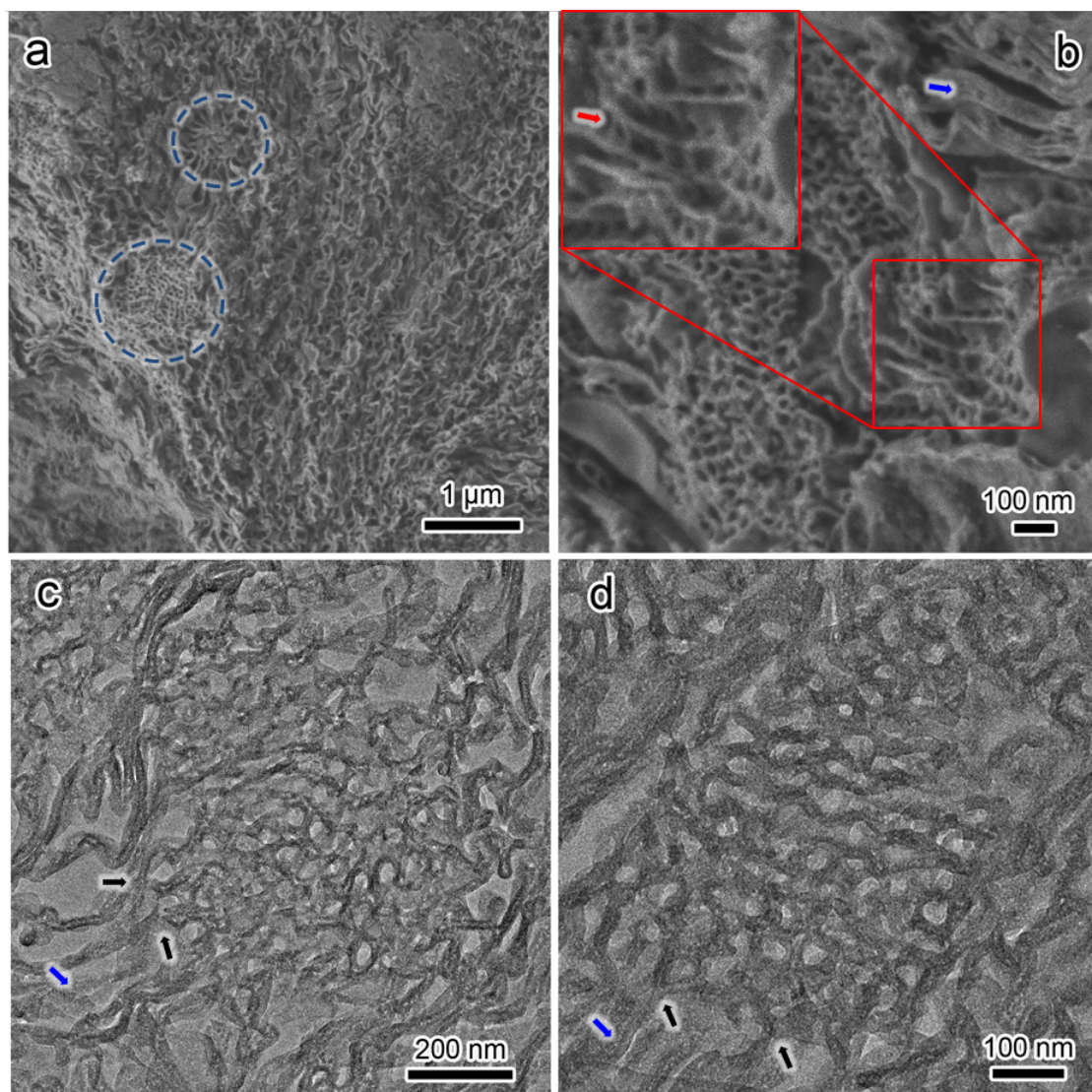


Figure 4. SEM and TEM images of MS-3. (a) Low-magnification SEM image of MS-3. (b) High-magnification SEM image of a transition center. (c, d) TEM images of the structural interconversion.

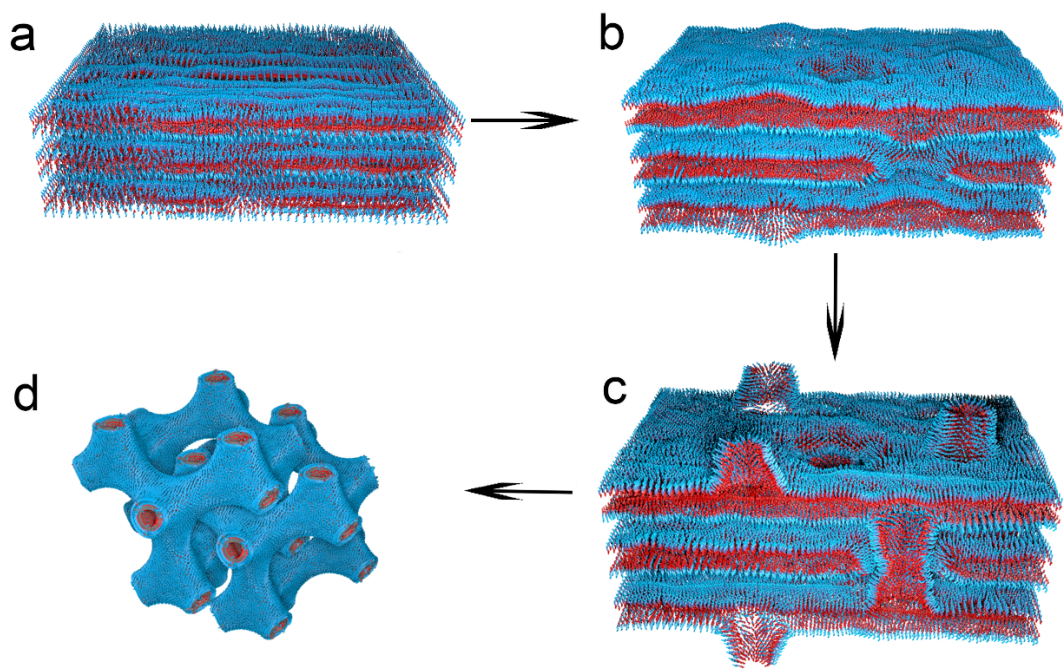


Figure 5. Schematic drawing of the structural transition between lamellar and bicontinuous DD structure. (a) Lamellar, (b) The formation of HPLs, (c) The formation of stalk between lamellar, (d) bicontinuous DD structure.